Nanotesla magnetoresistance in π-conjugated polymer devices

Philippe Klemm,[1] Sebastian Bange,[1] Agnes Pöllmann,[1] Christoph Boehme,[2] and John M. Lupton[1,*]

[1]*Institut für Experimentelle und Angewandte Physik, Universität Regensburg, 93040 Regensburg, Germany*
[2]*Department of Physics and Astronomy, University of Utah, Salt Lake City, Utah 84112, USA*

We demonstrate submicrotesla sensitivity of organic magnetoresistance in thin-film diodes made of the conducting polymer poly(styrene sulfonate)-doped poly(3,4-ethylenedioxythiophene) (PEDOT:PSS). The magnetoresistance sensitivity is shown to be better than 20 parts per billion (ppb). As for other conjugated polymers, magnetoresistance can be separated into two regimes of field strength: the nonmonotonic ultrasmall magnetic field effect on magnetic field scales below 2 mT, and the monotonic intermediate magnetic field effect on scales over several tens of mT. The former gives the PEDOT:PSS magnetoresistance curve a characteristic W-shaped functionality, with inverted turning points compared to those found in conventional organic light-emitting diode (OLED) devices. We succeed in resolving the ultrasmall magnetic field effect of the PEDOT:PSS layer incorporated within an OLED structure, which is responsible for an additional magnetoresistive feature on the ppm scale. Such a device shows unprecedented complexity in magnetoresistance with a total of four extrema within a field range of ± 1 mT. We propose that these unique characteristics arise from spin-spin interactions in the weakly bound carrier pairs responsible for the spin-dependent recombination probed in magnetoresistance.

Understanding and manipulating spin-pair correlations in conjugated polymer materials have proven to be the key to applications, such as in organic light-emitting diodes (OLEDs), polymer photovoltaics, or magnetometers based on polymers [1–7]. Magnetic-field-dependent measurements enable the study of effects relating to the ensemble spin statistics within a polymer film. For example, in magnetic resonance-type experiments, where coherent spin manipulation is achieved by applying oscillating magnetic fields to Zeeman-split sublevels of the charge-carrier pairs, the influence of hyperfine coupling on macroscopic properties such as conductivity has been established [4,8–10]. Such an experiment demonstrates the interplay between an external magnetic field and an internal field, the hyperfine field [11], and illustrates the interrelation between magnetoresistance and magnetic resonance when carried out under continuous-wave steady-state detection [11]. It has also been demonstrated that a further form of internal field—dipolar spin-spin interactions between the electron and the hole—can potentially modify ensemble spin statistics [12], even though these effects have generally been regarded as negligible in weakly bound charge-carrier pairs. Electronic spin-spin interaction effects are particularly pronounced in materials with weak hyperfine coupling strengths, such as in poly(styrene-sulfonate)-doped poly(3,4-ethylenedioxythiophene) (PEDOT:PSS) at low temperatures [12]. This material is proven as a stable and widely used hole injection layer in organic semiconductor devices [13], and has recently been the subject of renewed investigation in light of its remarkable Seebeck coefficient and associated thermoelectricity [14–16], as well as the pronounced inverse spin Hall effect [17]. Here, we show that PEDOT:PSS provides a model system to study the interplay of external, static magnetic fields and internal fields arising from spin-spin interactions within the charge-carrier pairs responsible for spin-dependent transport

and magnetoresistive effects in thin-film devices made of these materials. We demonstrate distinct magnetoresistive features on unprecedented scales of down to 20 parts per billion (ppb), more than an order of magnitude gain in sensitivity over prior studies [18]. Even though PEDOT:PSS was previously reported to possess no bulk magnetic-field effect [19,20], we demonstrate that both the ultrasmall magnetic-field effect [18,20–22]—a pronounced nonmonotonic W shape in the magnetoresistance below 1 mT—and the magnetoresistance at intermediate field strength generally attributed to the influence of hyperfine coupling [19,23] can be observed in a PEDOT:PSS device at room and liquid-helium temperature.

We studied the magnetoresistance of 120 nm thick PEDOT:PSS (Clevios P VP AI 4083) layers spin coated on prepatterned indium-tin oxide covered glass substrates, where the top contact was provided by thermally evaporated aluminum [see the left-hand inset in Fig. 1(a)]. The devices, with an area per pixel of 2.4 mm², were measured under a vacuum atmosphere (10^{-6} mbar) in a cold-finger cryostat and placed at the center of a solenoid coil that provided an external magnetic field of up to 60 mT orthogonal to the sample plane. The devices were operated under constant current from a Keithley 236 source-measure unit. The device voltage was measured by a Keithley 2002 multimeter [24]. At room temperature, current-voltage characteristics of such devices show effectively Ohmic behavior up to currents of several hundred µA, whereas they become nonlinear at higher currents and also at liquid-helium temperature [24]. After a minimum settling time of several minutes at constant current, multiple field sweeps were carried out in series and averaged over to eliminate slow drifts in the device resistance due to degradation effects [24]. Magnetoresistance signals are clearly discernible in each individual magnetic field sweep in all measurements reported, but averaging significantly improves the signal-to-noise ratio [24]. Figure 1(a) shows the relative magnetoresistance $\frac{\Delta R}{R} = \frac{R(B) - R(0)}{R(0)}$ of a PEDOT:PSS device at room temperature at a constant current of 5 mA as a function

───────────
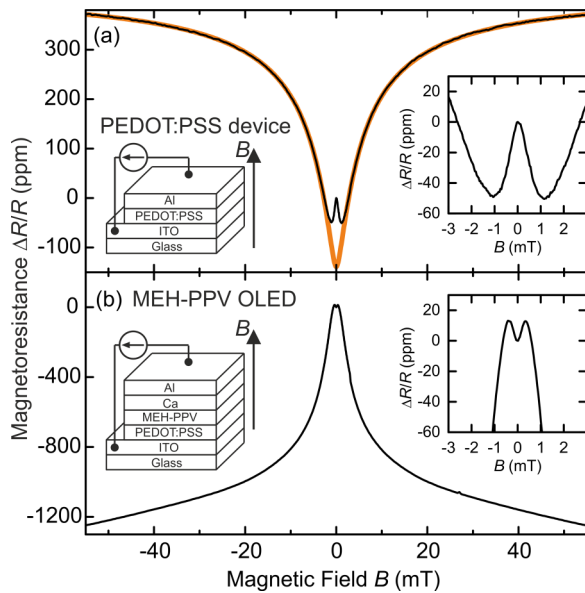*[*]john.lupton@ur.de

　　　　　　　　241407-1

FIG. 1. Magnetoresistance of polymer-based diodes under a constant current of $I = 5$ mA at room temperature. The left-hand insets show the device geometries and the relative orientation of the magnetic field and device stack schematically. (a) Magnetoresistance of a device structure incorporating only PEDOT:PSS as the active layer between two electrodes. A zoom into the ultrasmall magnetic field effect close to the origin is shown in the right-hand inset. The orange line is a fit of the outer data region to the function $f(B) \propto \text{const} + (\frac{B}{|B|+B_0})^2$, with B_0 the fitting constant. Because of the high conductivity of the PEDOT:PSS layer, the absolute resistance at zero field is quite low [$R_{(B=0)} = 119\,\Omega$]. (b) Magnetoresistance of a conventional OLED structure with PEDOT:PSS and MEH-PPV polymer layers [$R_{(B=0)} = 697\,\Omega$]. The right-hand inset, plotted on the same absolute scale as in (a), shows that the ultrasmall magnetic field effect is much weaker in this case. For both devices, the dominant magnetoresistive response occurs in the intermediate-field regime of several tens of mT. This effect is generally associated with hyperfine coupling [11].

of the magnetic field B. The magnetoresistance response of PEDOT:PSS at magnetic fields $|B| > 1$ mT is positive and follows the function $f(B) = \text{const} + (\frac{B}{|B|+B_0})^2$, one of two major recurring qualitative functionalities in the magnetoresistance of organic materials [23] with B_0 a fitting constant. The fit is shown by the orange line in Fig. 1(a). At magnetic fields $|B| < 1$ mT, a negative response is observed, i.e., the resistance decreases as a function of $|B|$. This response and the formation of a W shape of the magnetoresistive response around the field origin is telltale behavior of the ultrasmall magnetic field effect [21] and is depicted in more detail in the right-hand inset of Fig. 1(a). No significant change in the strength of magnetoresistance is observed upon increasing the thickness of the PEDOT:PSS layer to several microns by drop casting the material [24], indicating that the observed effect indeed relates to the bulk of the material and not an interface. For comparison, we examined the magnetoresistance of an OLED, utilizing PEDOT:PSS as the hole injection layer into an active layer of poly[2-methoxy-5-(2-ethylhexyloxy)-1,4-phenylenevinylene] (MEH-PPV), capped with a 10 nm electron injection layer of calcium and a 250 nm aluminum

top electrode, as sketched in the left-hand inset of Fig. 1(b). The relative magnetoresistance $\frac{\Delta R}{R}$ of the MEH-PPV OLED at room temperature and at a constant current of 5 mA, as depicted in Fig. 1(b), is in agreement with previous reports [20,21] and is clearly inverted compared to the PEDOT:PSS device.

The different signs of magnetoresistance of these two devices may be attributed to the charge-carrier balance within the devices [21]. The MEH-PPV OLED constitutes a bipolar device [25], containing roughly the same density of holes and electrons, and therefore exhibits a negative magnetoresistance signal, whereas the positive response of the magnetoresistance of the PEDOT:PSS device may be an indication of a single dominant charge-carrier species [21], as could be expected for such a highly doped material [26]. While recent results in electrically (i.e., conductivity) detected magnetic resonance (EDMR) spectroscopy of PEDOT:PSS device structures provided strong evidence for the presence of two oppositely charged carriers in the material at low temperatures [12], for the following discussion knowledge of the exact nature of the charge carriers involved in the magnetoresistive response is not necessary. Apart from the change in sign between the PEDOT:PSS device and the MEH-PPV OLED, it can be clearly seen that the absolute magnetoresistance of the MEH-PPV OLED reaches a value four times higher than that of the PEDOT:PSS device within the magnetic field range accessible in the experimental setup. In addition, the width of the magnetoresistance effect, usually defined as half of the full width at half maximum of the overall magnetoresistance trace between positive and negative fields [19], $\Delta B = (1 + \sqrt{2})B_0$, is broader for the PEDOT:PSS device with $\Delta B = 6.9$ mT than for the MEH-PPV OLED with $\Delta B = 4.8$ mT. We note, though, that ΔB is technically a qualitative metric serving as a guide only since neither magnetoresistance curve saturates fully. Since this width is generally related to the magnitude of hyperfine coupling [20], it appears to actually indicate a stronger hyperfine coupling in PEDOT:PSS at room temperature compared to MEH-PPV [21]. This, of course, seems surprising, since there are fewer protons present in PEDOT:PSS than in MEH-PPV and, as a consequence, the (low-temperature) EDMR spectrum of PEDOT:PSS is narrower than for MEH-PPV [12]. However, at the same time both the magnitude of the ultrasmall magnetic field effect, defined as the magnitude of the magnetoresistance at the slope's sign reversal, as well as the magnetic field where the sign reversal occurs, are four times higher in the PEDOT:PSS device than in the MEH-PPV OLED. On the one hand, one may expect the more delocalized carriers in PEDOT at room temperature to come closer to the remote protons and experience larger hyperfine interactions, and on the other hand, one could anticipate motional narrowing to give rise to the opposite effect. Given the blended nature of PEDOT:PSS, the interplay between these two competing effects does not appear trivial.

With careful sampling, the signature of the ultrasmall magnetic field effect of the PEDOT:PSS layer can also be observed in the magnetoresistance of an MEH-PPV OLED containing a PEDOT:PSS hole injection layer, albeit only at low temperatures. As shown in Fig. 2, the slope of the magnetoresistance of the MEH-PPV OLED at 4.5 K exhibits a
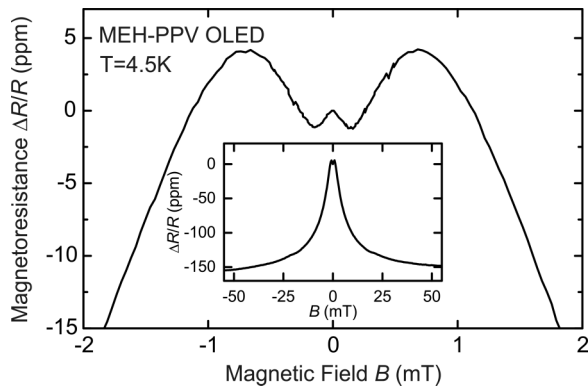
FIG. 2. Magnetoresistance of an MEH-PPV OLED under a constant current of 250 μA at liquid-helium temperature [$R_{(B=0)} =$ 34.5 kΩ]. On field scales of ± 1 mT a total of five extrema are observed, at $B_1 = 0$ mT, $B_2 \cong \pm 150 \mu$T, $B_3 \cong \pm 700 \mu$T, giving rise to a nonmonotonic double-W functionality. The magnetoresistance on field scales of up to 55 mT shows no unexpected changes in functionality, as displayed in the inset.

second sign reversal at a magnetic field of $\sim 150 \mu$T, giving rise to a *twofold* W functionality of the magnetoresistance sweep. We attribute this feature with a tiny amplitude of 1.2 parts per million (ppm) to the magnetoresistance of the PEDOT:PSS hole injection layer superimposed on the magnetoresistance of the MEH-PPV active layer. The characteristic magnetic field where the sign reversal of the slope of the ultrasmall magnetic field effect occurs is approximately 700 µT and therefore doubled in comparison to the room-temperature value. This observation of a temperature dependence of the ultrasmall magnetic field effect is in contrast to the previously reported constant values of magnetoresistance upon changes in temperature and electrical driving power of an OLED with an active layer of 2-methoxy-5-(2′-dioctyloxy) PPV [21]. The magnitude of the ultrasmall magnetic field effect in the MEH-PPV OLED is reduced by a factor of approximately 4 (to ~ 4.2 ppm) compared to the pure PEDOT:PSS device. The general functionality of the magnetic field effect at fields $|B| > 1$ mT observed at room temperature appears to persist, although the half width at full maximum ΔB is increased slightly to approximately 5.6 mT. Crucially, the overall magnitude of the magnetoresistance at 50 mT decreases by almost an order of magnitude compared to room temperature, as seen in the inset of Fig. 2 when compared to Fig. 1(b). This finding is in stark contrast to the previous claim that magnetoresistance amplitudes in both the ultrasmall-field and intermediate-field regions change by the same degree with temperature [21]. The data presented here are consistent with a scenario where the two magnetoresistance regimes of the MEH-PPV OLED arise from two distinct mechanisms.

Having shown that we can resolve the distinct intrinsic PEDOT:PSS magnetoresistance in an MEH-PPV OLED containing a PEDOT:PSS layer, we address the question of the ultimate sensitivity of magnetoresistance in PEDOT:PSS devices. Figure 3(a) shows the ultrasmall-field and intermediate-field magnetoresistance of such a device measured at a temperature of 4.5 K. In contrast to the magnetic field effect in the MEH-PPV OLED, the reduced temperature leads to a *narrowing* of the ultrasmall magnetic field effect in the PEDOT:PSS
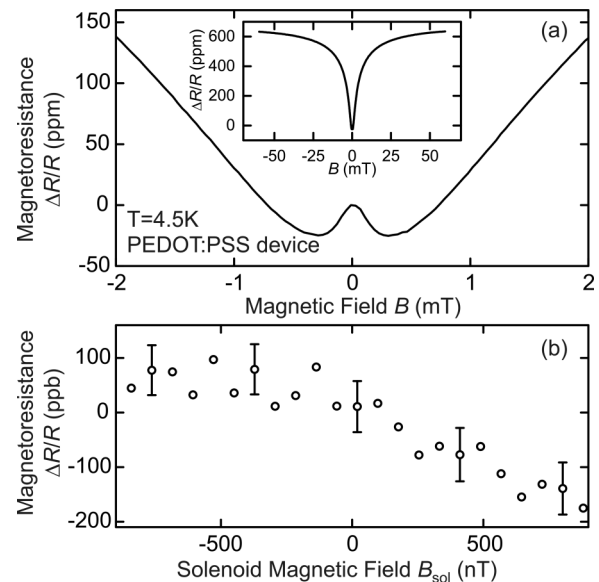

FIG. 3. Nanotesla magnetoresistance of PEDOT:PSS devices under a constant current of 250 μA at liquid-helium temperature [$R_{(B=0)} \sim 10$ kΩ]. (a) The ultrasmall magnetic field effect, shown in the ± 2 mT range, as a function of the total magnetic field $B = B_{\mathrm{sol}} + B_{\mathrm{earth}}$, where B_{sol} is the solenoid's magnetic field and B_{earth} is the local geomagnetic field. The inset shows the effect on higher magnetic field scales (± 60 mT). (b) High-resolution measurement, averaged over 300 consecutive sweeps of the solenoid field, showing an effective magnetic field sensitivity of ± 250 nT around the local geomagnetic field. Error bars indicate the standard error of the mean.

device with respect to room temperature. As shown in Fig. 3(a), the slope's sign reversal occurs at a magnetic field of 330 µT, less than half the value found at room temperature [see the inset of Fig. 1(a)]. The overall magnitude of the ultrasmall magnetic field effect changes only slightly from room temperature to 4.5 K, while the magnitude of the intermediate-scale magnetoresistance increases by a factor of 2. The half width at full maximum of the intermediate-scale magnetoresistance correspondingly drops substantially compared to room temperature, to $\Delta B = 4.7$ mT. Besides this temperature dependence, we also observe a change of inner and outer magnetoresistance functionalities of PEDOT:PSS devices with driving current, which we shall not discuss further here. Due to the strong reduction of the characteristic magnetic field scale of the ultrasmall magnetic field effect, the shape of the magnetoresistance curve becomes much steeper compared to other devices, such as the MEH-PPV OLED. This property allows for unprecedented sensitivity in steady-state magnetoresistance measurements as demonstrated in Fig. 3(b). A tuning of the solenoid magnetic field of ± 500 nT on top of the local geomagnetic field of $\sim 50 \mu$T leads to an observable change in the magnetoresistance of 100 ppb with a sensitivity of approximately 20 ppb. The polymer-based device is therefore able to detect magnetic field changes of less than one hundredth the geomagnetic field.

As in the case of the MEH-PPV OLED, because of the change with temperature in the ratio of the magnitude of the two magnetic field effects (on the ultrasmall- and intermediate-field scales), it is likely that different paramagnetic electronic

states are involved in these two distinct effects, if not even qualitatively different electronic mechanisms. Spin mixing mediated by the hyperfine interaction is thus unlikely to be the simultaneous origin of both the ultrasmall and the intermediate-scale magnetic field effects [21]. Aside from this model, three approaches to explain the origin of the ultrasmall magnetic field effect have been put forward: (i) a mechanism involving the zero-field splitting of the triplet-state polaron pair; (ii) the spin precession model; and (iii) electronic spin-spin interactions [21,27–29].

The first model (i) attributes the ultrasmall magnetic field effect to electron-hole triplet polaron pairs temporarily bound to a single charge carrier. These three charge carriers form either a spin-$\frac{1}{2}$ quartet or a spin-$\frac{3}{2}$ doublet state, whose temporal evolution in the external magnetic field emerges as a magnetic field effect on a macroscopic scale [27]. However, such a system has a very distinct signature in EDMR experiments, where the bound charge-carrier pairs are forced to oscillate between triplet states with the magnetic quantum numbers $m_s = 1, -1$, leading to a readily observable change in resistance under resonance. Since this effect has not been observed in EDMR spectroscopy of PEDOT:PSS devices at low temperatures [12], this mechanism is ruled out.

According to the spin precession model (ii) the presence of magnetoresistance at all field scales is determined by the hyperfine precession frequency of a charge-carrier spin in relation to the rate of exciton formation, which in more general terms is given by the charge-carrier hopping rate [28,30]. Within the data presented here, a set of model parameters can be found which reproduces the general trends of our results, neither confirming nor disproving this mechanism.

Spin-spin interactions (iii), i.e., the exchange and the spin-dipolar interaction, have been invoked not only in models for magnetoresistance in OLEDs [29,31], but are also utilized in the description of magnetic field effects in organic crystals and in spin chemistry in general [32,33]. Signatures of dipolar spin-spin coupling were recently resolved in the second harmonic of spin-Rabi flopping in pulsed EDMR experiments on PEDOT:PSS at liquid-helium temperature [12]. These interactions, while usually considered to be sufficiently small to be neglected in steady-state measurements, lift the degeneracy of the singlet and triplet manifolds of weakly coupled charge-carrier pairs at zero magnetic field [29]. Upon applying an external magnetic field, the Zeeman effect may energetically align specific triplet states with the singlet state of the carrier pair [32]. While aligned, mixing between singlet and triplet states may increase, inducing a macroscopically observable change in device resistance which is ultimately dominated by spin-dependent electron-hole recombination [29]. Specifically, stronger spin-spin interactions have been predicted to enhance the magnitude of the ultrasmall magnetic field effect and to shift the turning point in the characteristic W shape in magnetoresistance to higher fields [29]. Such a phenomenon may explain the behavior observed in the PEDOT:PSS device when raising the temperature from 4.5 K to room temperature. An increase in spin-spin interaction strength may indicate a closer proximity of the constituents of the charge-carrier pair at higher temperatures, in agreement with the prediction of more localized states at lower temperatures [34,35] as well as the larger Onsager Coulombic capture radius of carrier pairs.

While the above discussion regarding magnetic interactions is, strictly, independent of the nature of the carrier-pair species—whether bipolar polaron pairs or unipolar bipolarons—substantial work has evolved around explaining intermediate and ultrasmall magnetic field effects with the formation of bipolarons [28]. The fundamental difference between spin-dependent recombination (polaron pairs) and transport (bipolarons) is that only the former shows up in constant-current electroluminescence, a direct measure of recombination. At intermediate field strengths a rigorous quantitative comparison of electroluminescence-detected magnetic resonance (ELDMR) and EDMR leaves no room for spin-dependent transport, i.e., bipolarons, in MEH-PPV [36]. In the heavily doped PEDOT:PSS, one could anticipate bipolaron processes, but, again, at intermediate fields compelling evidence exists against this hypothesis: EDMR signatures of carrier pairs are quenched in PEDOT:PSS/MEH-PPV bilayer devices, implying that electron injection into the PEDOT:PSS layer is suppressed [12]. This observation appears to be in contrast to the additive effect of magnetoresistance in Fig. 2. We therefore cannot exclude a possible contribution of bipolarons to the low-field magnetoresistance of PEDOT:PSS.

Finally, we note that the fact that the intermediate-field-strength magnetoresistance effect becomes narrower in PEDOT:PSS films at lower temperatures (with ΔB decreasing from approximately 6.9 to 4.7 mT) is consistent with the carriers becoming more localized on the thiophene units of the PEDOT. At low temperatures, the magnetoresistance is narrower in PEDOT:PSS ($\Delta B = 4.7$ mT) than in MEH-PPV ($\Delta B = 5.6$ mT), implying weaker hyperfine coupling [20], which is to be expected for the thiophene units with reduced hydrogen content compared to phenylene-vinylene units. The behavior in magnetoresistance is therefore analogous to that found in EDMR of MEH-PPV and PEDOT:PSS [12].

While we are unable to determine the precise microscopic origin of the ultrasmall magnetic field effect discussed here, the occurrence of bulk magnetoresistance and its dependence on temperature sheds light on previously unconsidered characteristics of magnetic field effects on these magnetic field scales. Due to the remarkable strength of the ultrasmall magnetic field effect in PEDOT:PSS compared to the overall magnetoresistance effect at higher magnetic fields, i.e., the contrast of the W shape with respect to the overall magnetoresistance response, and the superposition of distinct magnetic field effects in polymeric bilayer structures, we expect further measurements over a wide range of experimental parameters such as temperature, current density, and chemical composition on these types of devices to provide a means of illuminating the origin of this effect. Magnetoresistance in organic conductors arises from spin-dependent carrier-pair processes [11] with striking similarity to radical-pair processes [37] which have been invoked to explain, among other things, magnetoception of some migratory bird species [38]. The underlying understanding is that miniscule perturbations in the magnetic field can alter the outcome of coherent electronic spin precession in reactive carrier-pair intermediates, which recombine to form singlet or triplet molecular excited states [39]. The demonstrated sensitivity of magnetoresistance on static magnetic field scales of less than one hundredth of the

Earth's field is amongst the highest sensitivity reported for carrier-pair (or radical-pair) processes to date. The nanotesla field scale is remarkably close to that invoked in the context of the sensitivity of migratory birds to ambient electromagnetic noise [39]. In avian photopigment-based magnetoreceptors, spin coherence times of hundreds of microseconds have been invoked to explain the observed sensitivity to geomagnetic field variations [37–41]. Since our devices show sensitivity to fields two orders of magnitude weaker than the Earth's field, one may speculate that even longer spin coherence times may be responsible for the observed effect. However, such long times have not been observed in direct measurements of spin coherence in organic semiconductors by electrically detected spin-echo spectroscopy, which typically yield pure decoherence times (T_2) of order 1 μs [42–44]. This discrepancy may be linked to the fact that EDMR measurements, such as spin-echo spectroscopy, solely monitor mobile resonant charge species, whereas it is precisely this hopping mobility of carriers in the inhomogeneous hyperfine fields which induces spin dephasing [42]. In contrast, quasi-steady-state magnetoresistance can also probe static (trapped) charge carriers and their influence on overall conductivity [45–47]. The spin coherence of trapped carriers may therefore be much longer than 1 μs. Finally, we note that the present experiments are limited by instrumental resolution as well as the slope of the initial magnetoresistance in the vicinity of the zero-field point. By using even more sensitive electrometers, we anticipate a further substantial gain in sensitivity. In addition, deuteration of the conducting polymer will reduce local hyperfine fields [11,20,21], further steepening the magnetoresistance curve and raising overall sensitivity.

[1] R. H. Friend, R. W. Gymer, A. B. Holmes, J. H. Burroughes, R. N. Marks, C. Taliani, D. D. C. Bradley, D. A. Dos Santos, J. L. Brédas, M. Lögdlund, and W. R. Salaneck, Nature (London) **397**, 121 (1999).

[2] D. Chaudhuri, E. Sigmund, A. Meyer, L. Röck, P. Klemm, S. Lautenschlager, A. Schmid, S. R. Yost, T. Vanvoorhis, S. Bange, S. Höger, and J. M. Lupton, Angew. Chem., Int. Ed. **52**, 13449 (2013).

[3] P. W. M. Blom, V. D. Mihailetchi, L. J. A. Koster, and D. E. Markov, Adv. Mater. **19**, 1551 (2007).

[4] W. J. Baker, K. Ambal, D. P. Waters, R. Baarda, H. Morishita, K. van Schooten, D. R. McCamey, J. M. Lupton, and C. Boehme, Nat. Commun. **3**, 898 (2012).

[5] V. A. Dediu, L. E. Hueso, I. Bergenti, and C. Taliani, Nat. Mater. **8**, 707 (2009).

[6] C. Boehme and J. M. Lupton, Nat. Nanotechnol. **8**, 611 (2013).

[7] S. L. Bayliss, A. D. Chepelianskii, A. Sepe, B. J. Walker, B. Ehrler, M. J. Bruzek, J. E. Anthony, and N. C. Greenham, Phys. Rev. Lett. **112**, 238701 (2014).

[8] S.-Y. Lee, S.-Y. Paik, D. R. McCamey, J. Yu, P. L. Burn, J. M. Lupton, and C. Boehme, J. Am. Chem. Soc. **133**, 2019 (2011).

[9] D. R. McCamey, H. A. Seipel, S.-Y. Paik, M. J. Walter, N. J. Borys, J. M. Lupton, and C. Boehme, Nat. Mater. **7**, 723 (2008).

[10] D. R. McCamey, K. J. van Schooten, W. J. Baker, S.-Y. Lee, S.-Y. Paik, J. M. Lupton, and C. Boehme, Phys. Rev. Lett. **104**, 017601 (2010).

[11] D. P. Waters, G. Joshi, M. Kavand, M. E. Limes, H. Malissa, P. L. Burn, J. M. Lupton, and C. Boehme, Nat. Phys. **11**, 910 (2015).

[12] K. J. van Schooten, D. L. Baird, M. E. Limes, J. M. Lupton, and C. Boehme, Nat. Commun. **6**, 6688 (2015).

[13] A. Elschner, S. Kirchmeyer, W. Lovenich, U. Merker, and K. Reuter, *PEDOT—Principles and Applications of an Intrinsically Conductive Polymer* (CRC, Boca Raton, FL, 2010).

[14] O. Bubnova, Z. U. Khan, A. Malti, S. Braun, M. Fahlman, M. Berggren, and X. Crispin, Nat. Mater. **10**, 429 (2011).

[15] O. Bubnova, Z. U. Khan, H. Wang, S. Braun, D. R. Evans, M. Fabretto, P. Hojati-Talemi, D. Dagnelund, J.-B. Arlin, Y. H. Geerts, S. Desbief, D. W. Breiby, J. W. Andreasen, R. Lazzaroni, W. M. Chen, I. Zozoulenko, M. Fahlman, P. J. Murphy, M. Berggren, and X. Crispin, Nat. Mater. **13**, 190 (2013).

[16] G.-H. Kim, L. Shao, K. Zhang, and K. P. Pipe, Nat. Mater. **12**, 719 (2013).

[17] K. Ando, S. Watanabe, S. Mooser, E. Saitoh, and H. Sirringhaus, Nat. Mater. **12**, 622 (2013).

[18] T. D. Nguyen, E. Ehrenfreund, and Z. V. Vardeny, Org. Electron. **14**, 1852 (2013).

[19] T. D. Nguyen, Y. Sheng, J. Rybicki, G. Veeraraghavan, and M. Wohlgenannt, J. Mater. Chem. **17**, 1995 (2007).

[20] T. D. Nguyen, G. Hukic-Markosian, F. Wang, L. Wojcik, X.-G. Li, E. Ehrenfreund, and Z. V. Vardeny, Nat. Mater. **9**, 345 (2010).

[21] T. D. Nguyen, B. R. Gautam, E. Ehrenfreund, and Z. V. Vardeny, Phys. Rev. Lett. **105**, 166804 (2010).

[22] J. Danon, X. H. Wang, and A. Manchon, Phys. Rev. Lett. **111**, 066802 (2013).

[23] Ö. Mermer, G. Veeraraghavan, T. L. Francis, Y. Sheng, D. T. Nguyen, M. Wohlgenannt, A. Köhler, M. K. Al-Suti, and M. S. Khan, Phys. Rev. B **72**, 205202 (2005).

[24] See Supplemental Material at http://link.aps.org/supplemental/10.1103/PhysRevB.95.241407 for more extensive details of the experimental setup, measurement procedure, averaging procedure and data analysis, complete measurement parameters, examples of current-voltage characteristics and signatures of non-Ohmic behavior, and examples of sample-to-sample variation.

[25] W. J. Baker, D. R. McCamey, K. J. van Schooten, J. M. Lupton, and C. Boehme, Phys. Rev. B **84**, 165205 (2011).

[26] A. J. Heeger, J. Phys. Chem. B **105**, 8475 (2001).

[27] T. D. Nguyen, T. P. Basel, Y. J. Pu, X. G. Li, E. Ehrenfreund, and Z. V. Vardeny, Phys. Rev. B **85**, 245437 (2012).

[28] A. J. Schellekens, W. Wagemans, S. P. Kersten, P. A. Bobbert, and B. Koopmans, Phys. Rev. B **84**, 075204 (2011).

[29] N. J. Harmon and M. E. Flatté, Phys. Rev. B **85**, 245213 (2012).

[30] S. P. Kersten, A. J. Schellekens, B. Koopmans, and P. A. Bobbert, Phys. Rev. Lett. **106**, 197402 (2011).

[31] W. Wagemans, A. J. Schellekens, M. Kemper, F. L. Bloom, P. A. Bobbert, and B. Koopmans, Phys. Rev. Lett. **106**, 196802 (2011).

[32] O. Efimova and P. J. Hore, Biophys. J. **94**, 1565 (2008).

[33] R. P. Groff, A. Suna, P. Avakian, and R. E. Merrifield, Phys. Rev. B **9**, 2655 (1974).

[34] L. Yang, D. Yi, S. Han, and S. Xie, Org. Electron. **23**, 39 (2015).

[35] Y. L. Zhang, X. J. Liu, and Z. An, Europhys. Lett. **111**, 17009 (2015).

[36] M. Kavand, D. Baird, K. van Schooten, H. Malissa, J. M. Lupton, and C. Boehme, Phys. Rev. B **94**, 075209 (2016).

[37] T. Ritz, S. Adem, and K. Schulten, Biophys. J. **78**, 707 (2000).

[38] K. Maeda, K. B. Henbest, F. Cintolesi, I. Kuprov, C. T. Rodgers, P. A. Liddell, D. Gust, C. R. Timmel, and P. J. Hore, Nature (London) **453**, 387 (2008).

[39] S. Engels *et al.*, Nature (London) **509**, 353 (2014).

[40] J. M. Cai and M. B. Plenio, Phys. Rev. Lett. **111**, 230503 (2013).

[41] E. M. Gauger, E. Rieper, J. J. L. Morton, S. C. Benjamin, and V. Vedral, Phys. Rev. Lett. **106**, 040503 (2011).

[42] W. J. Baker, T. L. Keevers, J. M. Lupton, D. R. McCamey, and C. Boehme, Phys. Rev. Lett. **108**, 267601 (2012).

[43] H. Malissa, M. Kavand, D. P. Waters, K. J. van Schooten, P. L. Burn, Z. V. Vardeny, B. Saam, J. M. Lupton, and C. Boehme, Science **345**, 1487 (2014).

[44] R. Miller, K. J. van Schooten, H. Malissa, G. Joshi, S. Jamali, J. M. Lupton, and C. Boehme, Phys. Rev. B **94**, 214202 (2016).

[45] M. Cox, P. Janssen, F. Zhu, and B. Koopmans, Phys. Rev. B **88**, 035202 (2013).

[46] M. Cox, M. H. A. Wijnen, G. A. H. Wetzelaer, M. Kemerink, P. W. M. Blom, and B. Koopmans, Phys. Rev. B **90**, 155205 (2014).

[47] N. J. Harmon and M. E. Flatté, J. Appl. Phys. **116**, 043707 (2014).